A Comprehensive Study on Long-Term Durability of Protective Epoxy Coatings for Electrified Roadways

Md Tareq Hassan[1][0009-0007-3027-8889], Samiul Alam[1][0000-0002-0033-0507], and Juhyeong Lee[1][0000-0001-9383-3869]

[1] Utah State University, Logan UT 84322, USA
juhyeong.lee@usu.edu

Abstract. Underground wireless power transmission (WPT) systems are susceptible to environmental threats such as high temperatures, water ingress, and mechanical impact from above-ground objects. Typical WPT systems electronics are safeguarded with civil-grade epoxy coating, thus it is imperative to assess the coating's durability in these extreme conditions. Among various environmental threats, this study is primarily focused on both experimental and numerical investigations on long-term water diffusion characteristics of civil-grade epoxy materials at various temperatures. A series of water diffusion tests were performed on the specimens made from two commercially available electronics casting epoxy materials at room (23°C) and high (50°C) temperatures. A sequentially coupled, multi-physics finite element (FE) model was developed to predict water diffusion-induced hydrothermal and subsequent mechanical damage in the epoxy materials. The FE model consisted of four sequentially coupled analyses: (1) heat transfer analysis, (2) water diffusion analysis, (3) swelling analysis from long-term water diffusion, and (4) low velocity impact (LVI) analysis. The numerical results show good agreement with in-house experimental findings, indicating that the framework can serve as a baseline for predicting epoxy coating performance on WPT systems.

Keywords: Protective epoxy coating, Water Diffusion, Coupled Simulation.

1 Introduction

Wireless power transmission (WPT) refers to the technique that transfers electrical power by utilizing electromagnetic fields (EMF) without the need for physical connections. Its applications have become extensive in recent decades, encompassing the charging of mobile phones, implanted medical equipment, home appliances, and electric vehicles (EVs) [1]. A typical WPT system consists of a power source, transmitter coil, communication, and control systems. In the field of charging EVs, the WPT system can be categorized into two groups: (1) static, which requires the vehicle to remain stationary and (2) dynamic, which allows the vehicle to be charged while in motion [1]. In feasibility studies, dynamic WPT systems showed their capability to offer unlimited range and an emerging field of research for sustainable mobility of EVs [2]. For successfully transmitting the power from the underground WPT to moving vehicles,

uninterrupted functioning of the system and communication between them is required. However, the functions and communications can be affected by both environmental (e.g., water, high temperatures, soil corrosion) and mechanical (e.g., vehicles passing over, impact from falling objects) loadings. The main source of water in the soil under the highways is rainfall, where water can severely impact underground wireless communication systems by disrupting antenna return, bandwidth, and propagation path [3]. In addition, water leakage inside the electrical system can lead to the failure of capacitors, transistors, and printed circuit boards (PCB) by dielectric loss due to water intrusion, dendrite growth, creep corrosion, delamination, and leakage current [4–7]. Thus, diffusion through the underground WPT components can lead to the system's premature failure and frequent maintenance, which is a big concern in the sustainable application of dynamic WPT.

In commercial practice, to protect electronics from water, casing materials are used. Materials with lower permeability are chosen as casing for electronics [8]. Metals, glass, and ceramics exhibit lower permeability than polymers due to their densely packed atoms which cause them to be heavier in weight [9, 10]. Glass and ceramics are too fragile to be used as the casing materials of underground WPT, on the other hand some enclosing metals, such as iron and aluminum are vulnerable to corrosion and noble metals are too costly to be used. Potting of enclosing metals can be a solution to protect both enclosing structures and internal electronics. Polymeric materials (i.e., urethane, silicone gels, and epoxy) are widely used as potting materials [11].

The potting materials should be chosen based on adhesion to the metal casing, heat resistance capability, chemical inertness, and hygroscopic tendencies. Epoxies show better adhesion to metals than urethane and silicone. In addition, they have higher glass transition temperature (T_g), modulus, and strength than urethane [12–14]. Epoxy material typically possesses superior overall properties over urethane and silicone coatings. However, in addition to high water absorption (2-7%), the mechanical and structural performance of common polymer coatings (e.g., epoxy, acrylonitrile-butadiene-styrene, urethane) is significantly influenced by long-term hydrothermal aging [15-17]. As water molecules start to penetrate inside the polymer chains of the epoxy, it may lead to the plasticization of the material, affecting the mechanical properties and lowering T_g. Consequently, the maximum allowable working temperature of the epoxy is reduced. Furthermore, internal heat generation from the WPT system may cause the absorbed water to evaporate, leading to the development of internal vapor pressure. This can potentially soften the epoxy coating, making it more susceptible to swelling and internal damage [18–20]. Though moderate plasticization can improve the impact resistance/fracture toughness of the epoxy by preventing crack propagation, impact damage may allow more routes for water to penetrate the epoxy layers thus degrading its properties over time [21, 22].

A higher diffusivity and water uptake are seen when the epoxy materials are subjected to higher temperatures along with long-term diffusion [23]. If the temperature is higher than the T_g of the epoxy material, the maximum water saturation may increase significantly [24]. Thus, it is essential to understand the epoxy materials' inherent property changes and their contribution to long-term hydrothermal aging for their use in underground WPT systems. This long-term hydrothermal aging can degrade epoxy

materials, potentially allowing water to enter the WPT components. As a result, it is the most significant purpose of the epoxy to reduce water diffusion through it. Experimentally determined water diffusion parameters (i.e., saturation time, diffusivity, and solubility) of the epoxy material can help to predict how far water might travel in fully saturated epoxies before reaching the WPT system.

This research explores two commercially available electronics casting epoxy materials as coating layers for WPT systems. As these epoxies can be exposed to hydrothermal aging environments (water ingression at various temperatures) and low velocity impacts (LVI), it is critical to assess the coatings' performances. Water diffusion experiments at room (23°C) and high (50°C) temperatures were performed on the epoxy specimens to understand their long-term durability and performance in water environments. To predict their responses to both environmental aging and LVI threat, a sequentially coupled multi-physics numerical framework is developed and validated with in-house experimental tests. The numerical framework considered the effect of internal heat generation from the WPT components on the epoxy specimen. Afterward, mass diffusion and static analysis were subsequently coupled to understand its water absorption and swelling. Finally, an LVI simulation was coupled with the previous analyses to determine the residual performance of the epoxy specimen. This work proposes a novel modeling framework for epoxy coating materials, which can determine their residual structural performance after the combined effects of heat and water diffusion. This framework can be utilized for the selection of appropriate electronics casting materials for underground WPT systems by eliminating the need for complex and expensive experiments.

2 Experimental Procedure

2.1 Materials and Sample Preparation

The epoxy specimens employed in this work were 832FX and 832TC, supplied by M.G. Chemicals Ltd. Both epoxies are two-part potting compounds (part A-epoxy resin and part-B hardener) and commonly used for the protection of circuit boards and electronic assemblies. The chemical composition and material properties of each epoxy material can be found on the manufacturer's website [25]. The epoxy specimens were prepared by mixing the two-part potting compounds of each epoxy with a weight fraction of 1.1:1 [25]. Then the mixture was thoroughly stirred and sat for 15 minutes to de-air the mixture. After that, the mixture was poured into a silicone mold and cured at 65°C for 2 hours according to the manufacturer's suggestions [25]. The FX specimen has lower T_g (8.8℃) than the TC specimen (50℃). These T_g values make the FX specimen flexible and the TC specimen rigid after curing [25]. The cured epoxy samples were cut into specimens with the nominal dimensions of $190.5 \times 95 \times 5$ mm^3. The two epoxy specimens after curing and those prepared for water diffusion and LVI tests are shown in Fig. 1.

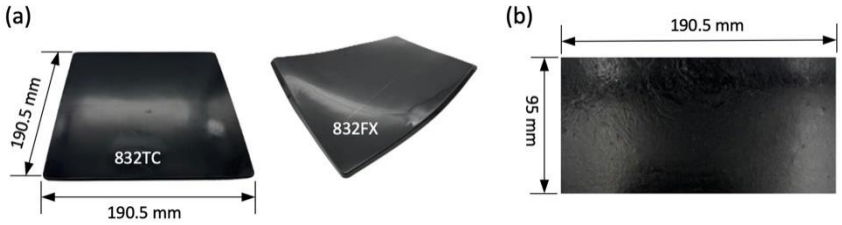

Fig. 1. Epoxy specimens (a) after curing and (b) cut into specimen size for water diffusion tests.

2.2 Water Diffusion Test Setup

Water diffusion tests were carried out in the water bath of tap water following ASTM D570-98 standard [26]. A total of 30 epoxy specimens were prepared for all epoxy specimen configurations (i.e., rigid (TC- 9 specimens) and flexible (FX- 6 specimens)) at room (RT) and high temperatures (HT) respectively. Figure 2 shows the water diffusion test set up in two different environmental conditions. During the test, the specimens were extracted and wiped off with a dry towel, and their weights were measured once every two days in the first month and weekly in the second month. The test continued until three consecutive weight measurements recorded an average water gain in a mass of no more than 1%, in accordance with the standard [26]. The change in weight (M_t) at any time t of a specimen due to water diffusion was determined using Eqn. 1.

$$M_t(t) = \frac{W_t - W_0}{W_0} \tag{1}$$

where W_t is the sample weight at any time t, and W_0 is the initial sample weight.

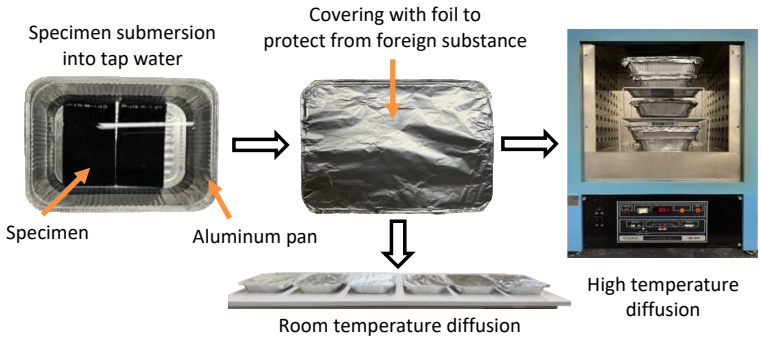

Fig. 2. Experimental setup in room temperature (RT) and high temperature (HT) diffusion.

3 Water Diffusion Test Results

Figures 3a and 3b each show the time evolution of water absorption (M_t in Eqn. 1) and the maximum water saturation level of FX and TC epoxy specimens under RT and HT diffusion conditions. The specimen's weight increments from the water diffusion

experiments were recorded for ~71 days and plotted with respect to the square root of time, thus ~ 41 hr in the x-axis of Fig. 3a corresponds to ~1704 hr in the actual diffusion experiment. Plotting the water absorption against 'time' or 'square root of time' is standard approach. The 'square root of time' unit is a widely accepted approach since the slope of the linear portion from the plot can then be used to estimate the diffusion coefficient.

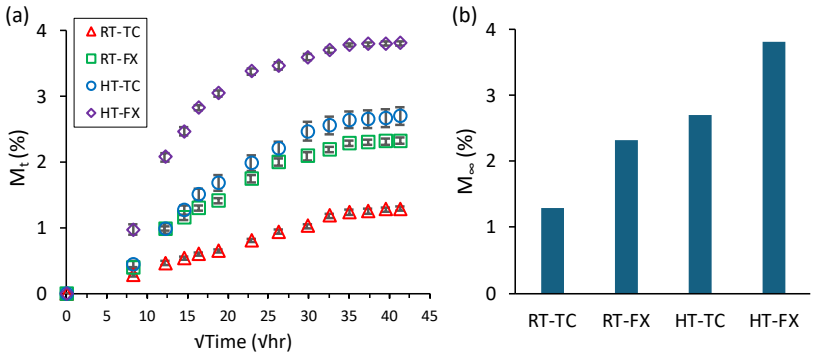

Fig. 3. (a) Specimen weight change M_t (%) over time and (b) maximum water saturation level M_∞ (%) of rigid (TC) and flexible (FX) epoxy specimens subjected to room temperature (RT) and high temperature (HT) diffusion.

As the specimens reached saturation, the FX specimens, which could be easily deformed in RT conditions due to weaker intermolecular bonds, demonstrated greater water absorption rates. FX specimens absorbed slightly more water (2.3%) compared to the TC specimens (1.3%) in both diffusion conditions. The relatively weaker intermolecular bonds in FX specimens allowed more water to penetrate the molecular network of the specimens. In the HT diffusion condition, both epoxy specimens had higher maximum water absorption levels than RT diffusion with higher absorption rates. The increased molecular distance between the cured epoxy molecules at high temperature allowed more water to be stored in the specimens compared to RT diffusion. In the case of the TC specimen, its water absorption almost doubled in HT diffusion, i.e. 1.3% to 2.7% due to the influence of temperature, which is also similar for the FX specimens. Among all material and testing configurations, the FX specimen at HT diffusion exhibited the highest maximum water absorption of ~3.8%, while the TC specimen at RT diffusion exhibited the least maximum water absorption of ~1.3%.

The diffusion temperature significantly influenced the physical state of the specimens over the course of hydrothermal aging. In the RT condition, the diffusion process did not result in any noticeable physical distortion in the specimens. However, during HT diffusion, as depicted in Fig. 4, the TC specimens exhibited warpage, which became increasingly pronounced towards the end of the diffusion period. The diffusion temperature (50 °C) was similar to the TC specimen's T_g (50 °C) [25], making them malleable after water diffusion. Furthermore, the water bath created non-uniform heating despite constant oven temperature. The specimen's bottom face got heated faster than the other faces as a result of direct contact with the bath pan. Additionally, the larger surface area of top and bottom faces compared to side faces led to higher heat flow rates on these

surfaces. Overall, these phenomena created non-uniform heat distribution in the specimen, and the malleability of the TC specimens allowed them to bend, which eventually became permanent over the long diffusion period. However, due to their significantly low T_g (8.8 °C) [25], the FX specimens were already malleable before undergoing diffusion. Consequently, despite being subjected to uneven heat distribution, they did not maintain their distorted shape after the water diffusion test. Overall, the FX specimens experienced a decrease in stiffness as a result of water molecules breaking the polymer chains throughout the diffusion.

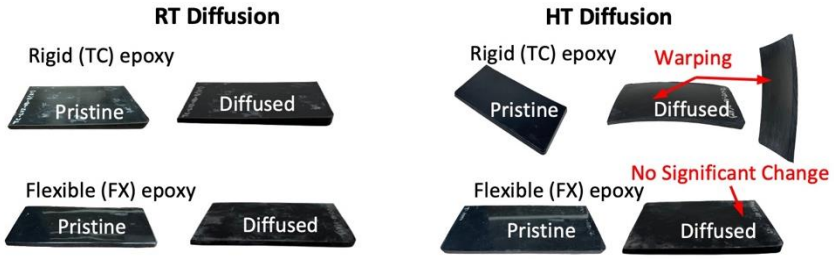

Fig. 4. Effect of water diffusion temperature on physical deformation of epoxy specimens.

4 Numerical Study

The epoxy coating can experience generated heat from the WPT and diffusion from surrounding water, causing it to swell due to high temperature and water content inside, and be subjected to impacts from external objects. A numerical study was carried out using ABAQUS to simulate their combined effects on the epoxy specimen [27]. The proposed finite element (FE) model consists of four sequentially coupled analyses to simulate water diffusion, swelling of the epoxy specimens, and LVI. *First*, transient heat transfer simulation was performed with the DFLUX subroutine to incorporate the effect of internal heat generation from the WPT system. Thermal properties (i.e., conductivity, coefficient of thermal expansion (CTE), and specific heat) of the epoxy specimen were defined as the input parameters in this simulation. *Second*, the water diffusion behavior of epoxy specimens was determined by using mass diffusion analysis. The specimens' water diffusion parameters and nodal temperatures from the heat transfer analysis were defined in the diffusion simulation as input parameters and predefined fields. *Third*, a static general analysis was performed with the UEXPAN subroutine to determine water-induced material swelling resulting from hydrothermal aging. The elastic properties (i.e., Young's modulus and Poisson's ratio), CTE, solubility, and coefficient of moisture expansion (CME) properties were required in the analysis. The UEXPAN subroutine was introduced to capture the combined hydrothermal expansion due to temperature distribution and water absorption. *Lastly*, a dynamic explicit analysis was performed to determine the residual structural performance of the epoxy specimen under LVI.

4.1 Transient Heat Transfer Analysis

The epoxy specimens might be subjected to heat generation from the underneath WPT system. To simulate the generated heat, a nonlinear transient heat transfer analysis was performed for both epoxy specimens. Table 1 lists the thermal properties of the epoxy specimens used in the heat transfer analysis [25].

Table 1. Thermal properties of epoxy specimens.

Specimen	Thermal conductivity (W/m/K)	CTE (ppm/°C)	Specific heat (J/g°C)
FX	0.3	218	0.80
TC	0.7	114	0.30

Using the DFLUX subroutine, a moving heat flux of 1000 W/m² was simulated over the specimen's bottom surface, moving in the longitudinal direction at 1.78 mm/s with a 10 mm radius. The heat transfer simulation was performed for 100 seconds. Note that, while the magnitude of heat flux and time duration were used as reference values, further investigation is needed to determine the actual parameters for internal heat generation in WPT components. Following a mesh sensitivity study, a global element size of 2 mm was chosen for the analysis, resulting in 13,680 three-dimensional (3D) linear hexahedral heat transfer elements (DC3D8 in ABAQUS). Figure 5a shows the FE mesh with the heat flux applied on the bottom surface of the model. A uniform initial temperature of 23°C was considered. Figures 5b and 5c each show the nodal temperatures in the FX specimen at 2 and 100 second of heat transfer simulation. From the temperature distribution contours, a circular-shaped heated area is seen on the specimen. The FX and TC models, when subjected to 1000 W/m^2 heat flux, showed the maximum temperatures of 29.8°C and 28.1°C, respectively.

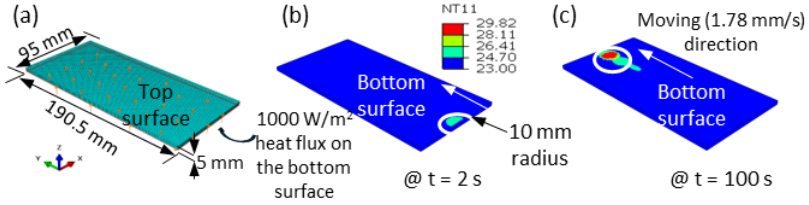

Fig.5. (a) FE model with heat flux loading, nodal temperatures in the FX specimen at time *t* at (b) 2 s, and (c) 100 s during the heat transfer simulation.

4.2 Water Diffusion Analysis

In general, the water absorption characteristics of polymeric materials are described using the Fickian diffusion model [28]. According to the model, water is transferred into a polymer only by diffusion, which is the movement of water from a region of higher concentration to a region of lower concentration. The Fickian diffusion model is built into ABAQUS, where the diffusion process is controlled based on the normalized

concentration [27]. The water diffusion in polymeric materials can be described by Fick's diffusion equation [28], as follows:

$$\frac{\partial C}{\partial t} = D\left(\frac{\partial^2 C}{\partial x^2} + \frac{\partial^2 C}{\partial y^2} + \frac{\partial^2 C}{\partial z^2}\right) \tag{2}$$

where C is the concentration, t is the time and D is the water diffusivity of a material. Equation 2 is the 3D Fickian model for isotropic material (i.e., $D_x = D_y = D_z = D$). The solution of the Fick's diffusion equation (Eqn. 2) can be determined as,

$$C = \frac{M_t}{M_\infty} = 1 - \frac{8}{\pi^2}\sum_{i=0}^{\infty}\frac{1}{(2i+1)^2} exp^{\left(\frac{-(2i+1)^2\pi^2 D_n t}{{h_n}^2}\right)} \tag{3}$$

where C is the concentration, M_t is the water absorption at time t (Fig. 3a), M_∞ is the maximum water saturation level (Fig. 3b), D_n and h_n each are the water diffusivity and thickness of a material.

The water diffusivity D_n was determined for the FE diffusion model by fitting the analytical model (Eqn. 3) to the experimental data. An in-house MATLAB code was developed to determine D_n and the predicted maximum water saturation level (M_∞). Figure 6 shows the fitted curve from the analytical model (Eqn. 3) with the experimental data for each epoxy specimen configuration. The water diffusion parameters obtained from the experiments are summarized in Table 2. The fitted parameters were used in the model to predict the water diffusion behavior of the epoxy specimen.

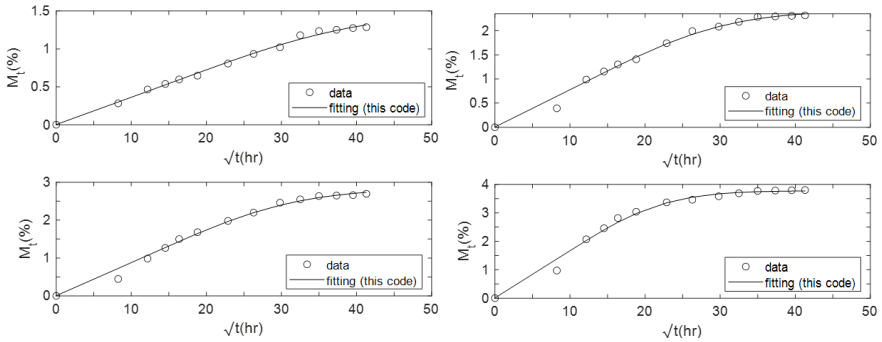

Fig. 6. Water diffusion results fitted with 1-D Fick diffusion model.

Table 2. Diffusion parameters obtained from 1-D Fick fitted diffusion model and comparison with the experimental value.

Specimen	Predicted/fitted value		Experimental value
	D (mm^2/hr)	M_∞ (%)	M_∞ (%)
RT-TC	0.0029	1.49	1.29
RT-FX	0.0051	2.41	2.32
HT-TC	0.0047	2.83	2.70
HT-FX	0.0096	3.78	3.80

A water diffusion model was developed and sequentially coupled with the previous heat transfer model to capture the water diffusion analyses for both specimens in RT and HT conditions. Note that, in ABAQUS, heat transfer element can be used in mass diffusion analysis. Thus, the global element size and type used in the water diffusion analysis were kept the same as the previous heat transfer model [27]. A total diffusion period of 1704 hours (~71 days) was simulated as motivated by the actual water diffusion test period. When applied on the WPT as a coating layer, only the top surface of the epoxy will be in contact with water. To simulate the actual water diffusion condition, the normalized concentration (i.e., φ is the ratio of concentration and solubility) boundary condition (φ = 1) was set at the top surface of the specimen and (φ = 0) was set at the bottom surface to create a through-the-thickness diffusion process. After that, the nodal temperatures from the previous heat transfer model were incorporated into the diffusion model as the predefined field. To simulate both RT and HT diffusion conditions, the diffusion process was modeled at two different temperatures (23 and 50°C).

4.3 Swelling Analysis

Swelling analysis was performed to characterize long-term water diffusion induced hydrothermal aging of the epoxy material. As the predefined fields of this analysis, the normalized nodal concentration (NNC) and nodal temperature fields from the previous water diffusion simulation were incorporated. All model parameters were kept identical to those of the water diffusion model, except for the element type: solid linear hexahedral elements (C3D8 in ABAQUS) were used in the swelling analysis to determine hydrothermal strains in the model. As motivated by physical boundary conditions, the bottom surface was made 'fixed' in the analysis. An UEXPAN subroutine was adopted to calculate the incremental strains as a function of NNC and nodal temperatures. Total expansion due to hydrothermal strains *expan* was calculated in the subroutine and updated during the analysis, i.e.,

$$expan = \alpha \times \Delta T + S \times \beta \times NNC \tag{4}$$

where α is the CTE; ΔT is the temperature difference; S is the solubility; β is the CME. Table 3 lists all material parameters used in the swelling simulation. Note that solubility is defined as the maximum quantity of a substance that can be dissolved in another substance and thus is equal to M_∞ in this work. The CME values are taken from Teverovsky et.al [29] and other parameters are provided in the manufacturer's website [25].

Table 3. Material parameters used in the swelling analysis.

Specimen	Density (Kgm-^{3})	Young's modulus (MPa)	Poisson's ratio	α (ppm/°C)	β (%/%)	S
RT-TC	1700	2850	0.30	114	0.18	0.015
RT-FX	1100	2.60	0.35	218	0.26	0.024
HT-TC	1700	2850	0.30	114	0.18	0.028
HT-FX	1100	2.60	0.35	218	0.26	0.038

4.4 LVI Analysis

An LVI simulation was performed after the swelling simulation to determine the residual structural performance of the epoxy specimen after swelling. In the model development, the part dimension, element size, and number were kept the same as in the previous analyses, except for element type. Solid linear hexahedral elements with reduced integration and hourglass control (C3D8R in ABAQUS) were chosen for this analysis. A hemispherical impactor with a 16 mm diameter was modeled as a discrete rigid part with an inertia of 4.92 kg at the center of mass of the hemisphere. In this work, a 3J impact energy was applied to the simulated model. Note that a series of LVI tests is required to determine the critical impact energy to provide an in-depth understanding of the dynamic failure of the epoxy specimen after water diffusion. An initial velocity of 1.1 m/s was assigned to the impactor to create the 3J impact energy. As boundary conditions, the four sides of the specimen were encastred and the impactor was made to translate only in the impacting direction. An approximate global element size of 1 mm was applied to discretize the impactor with bilinear rigid quadrilateral elements (R3D4 in ABAQUS). Figure 7 shows the boundary conditions of the LVI simulation.

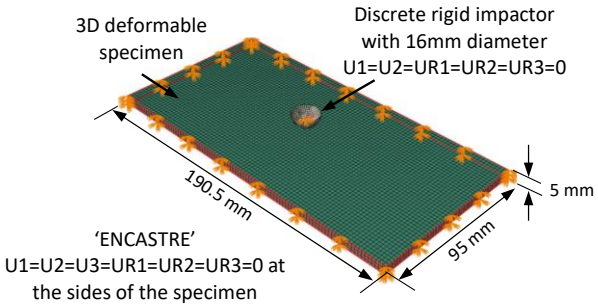

Fig. 7. Boundary conditions applied in LVI simulations.

5 Numerical Model Prediction

5.1 Water Diffusion Prediction

Figure 8 shows the NNC contours of the specimens at four distinct diffusion periods. The experimental findings indicated that water diffusion saturated after 1704 hr, so the diffusion process was simulated for the same time frame. The NNC contours depict the water intrusion in the thickness direction of the specimen, where the top surface of the specimen is exposed to water. Comparing the RT and HT diffusions, the FX and TC specimens both showed higher diffusion rates and concentration in HT diffusion. The FX specimen exhibited an early saturation with higher water concentration compared to the TC specimen, which corresponds to the experimental findings. Although the initial diffusion rate was higher in the FX specimen, the diffusion rate decreased as the specimen approached saturation, which led to a smaller difference in overall concentration between the TC and FX specimens. After the diffusion was concluded, the traveled distance of the water through the thickness was comparable in both specimens.

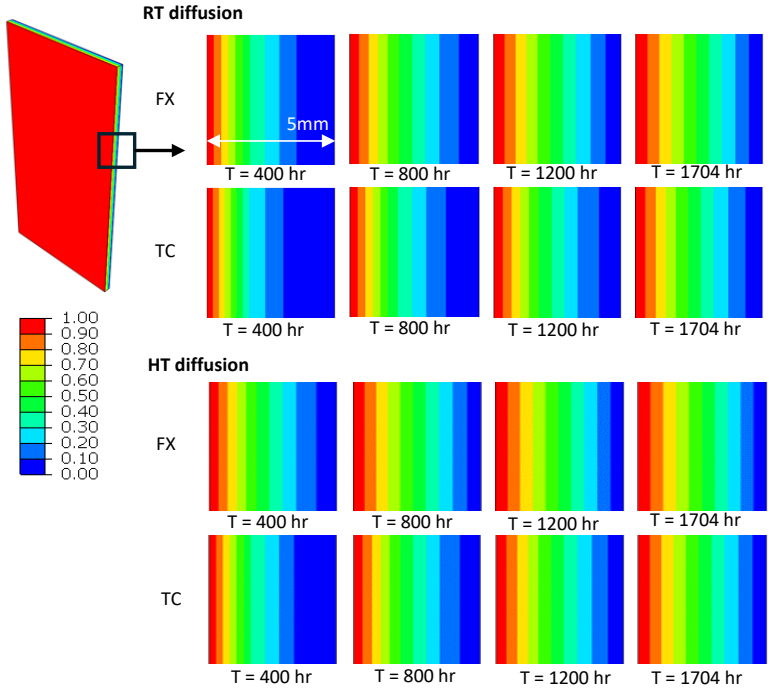

Fig. 8. Predicted NNC in the specimens at 400, 800, 1200, and 1704 hr at room temperature (RT) and high temperature (HT) diffusion conditions.

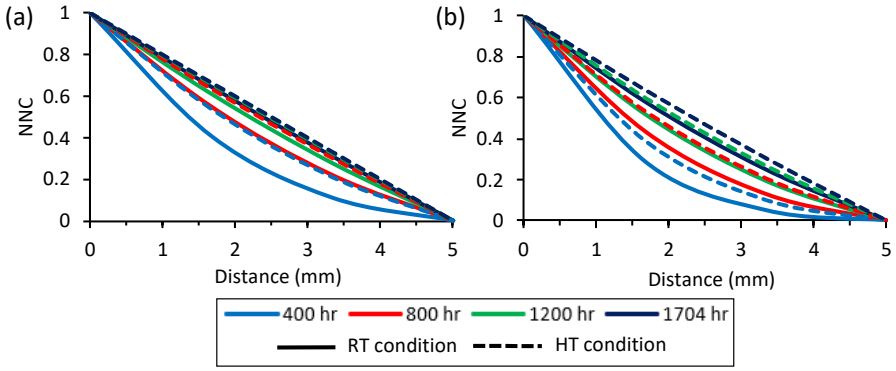

Fig. 9. Predicted normalized nodal concentrations (NNC) in the thickness direction of (a) FX and (b) TC specimens in room temperature (RT) and high temperature (HT) diffusion.

Figures 9a and 9b each demonstrate the NNC variation from the top surface to the bottom surface at four equidistance locations (i.e., 0, 1.67, 3.33, and 5 mm) of the FX and TC specimen, respectively. For both specimens, the internal water concentration is higher in the HT condition than in the RT condition in all locations. In HT diffusion, the FX specimen displayed no significant change in the water concentration after ~800 hr, which indicates that the specimen reached saturation. In RT diffusion, in contrast,

the FX specimen began to saturate after ~1200 hr. The HT condition also accelerated the diffusion rate of the TC specimen. For instance, the NNC in HT after ~1200 hr was higher than the NNC in RT diffusion after ~1704 hr. However, the NNC of TC specimen in HT had a slower increase compared to the FX specimen, which continued till the end of the diffusion process.

5.2 Swelling Prediction

Figure 10 shows overall hydrothermal strain fields in the epoxy specimens exposed to RT and HT diffusions. As previously mentioned, the bottom surface of the specimen was fixed. As a result, both specimens expanded the most at the top surface. From the strain fields, the effect of temperature in diffusion induced swelling prediction is seen on the top surfaces of both specimens. Both specimens expanded the most in HT diffusion i.e., the maximum total strain increased from 1.1% to 1.7% and 0. 4% to 0.8% in the FX and TC specimens respectively. High temperature allowed both specimens to achieve greater water molecular mobility which is the reason behind swelling more in HT condition. The temperatures in both RT and HT diffusion conditions were above the T_g of the FX specimen (8.8°C). As a result, the FX specimen became malleable/flexible before diffusion. After diffusion, it absorbed more water due to weaker inter-molecular bonds in the polymer chains than the TC specimen. Finally, the FX specimen swelled about two times the TC specimen in both diffusion conditions.

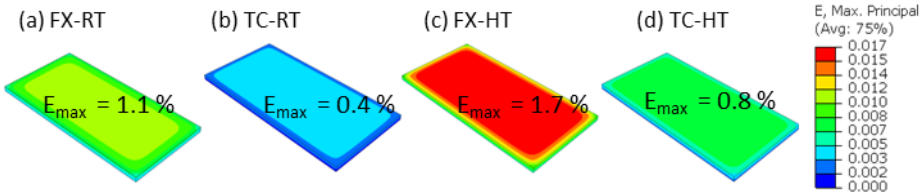

Fig. 10. Predicted total hydrothermal strains in the FX and TC specimens due to room temperature (RT) and high temperature (HT) diffusions.

5.3 LVI Prediction

The LVI numerical models were developed to predict the residual structural performance of both epoxy specimens after diffusion. To compare the effects of water diffusion and corresponding swelling in the specimens, the LVI responses of the epoxy specimens before and after water diffusion were compared. In this work, the LVI simulations were performed only with the available elastic properties (Table 3). As a result, the specimens were considered as fully elastic materials that recovered the energies after the impacts. So, this model could not capture any internal damage and energy absorption by the specimens from a 3J impact.

Figure 11 compares the predicted energy-time and load-displacement responses of the FX and TC specimens, respectively. As both specimens were modeled with only the elastic properties, there were no loops formed in the load-displacement curves, resulting from zero (calculated) absorbed energy. In this work, the residual performance of the epoxy specimens was compared based on peak force and peak displacement (Fig. 11). As for the FX specimen, water diffusion, regardless of RT and HT, did not affect

the residual LVI performance. The FX specimen had the same peak force (168 N) and peak displacement (43 mm) before and after water diffusion. However, the TC specimen exhibited a decrease in the peak force for both RT and HT diffusions. For instance, the pristine TC specimen had a peak force of 1,878 N which decreased to 1,846 N in RT and 1,798 N in HT diffusion. The peak displacements slightly increased after water diffusion. The peak displacement of the TC specimen was 3.7 mm in pristine condition, and it increased to 3.8 and 4.0 mm in RT and HT conditions, respectively. This model prediction suggests that the structural degradation associated with the microstructural change of the TC specimen was due to diffusion. The TC specimen exhibited a significantly higher peak force compared to the FX specimen, resulting in increased vibrations of the impactor, which can be observed as higher oscillations in the load-displacement curve of the TC specimen (Fig. 11). Additionally, the model predicted that the FX specimen experienced lower peak forces and larger displacements. This allowed the FX specimen to dissipate the impact energy more gently throughout its structure, reducing the likelihood of local damage. In contrast, the TC specimen encountered higher peak forces and low displacements, increasing the possibility of local damage. Therefore, it can be suggested that the FX epoxy is more suitable for reducing the severity of damage to WPT components when subjected to LVI.

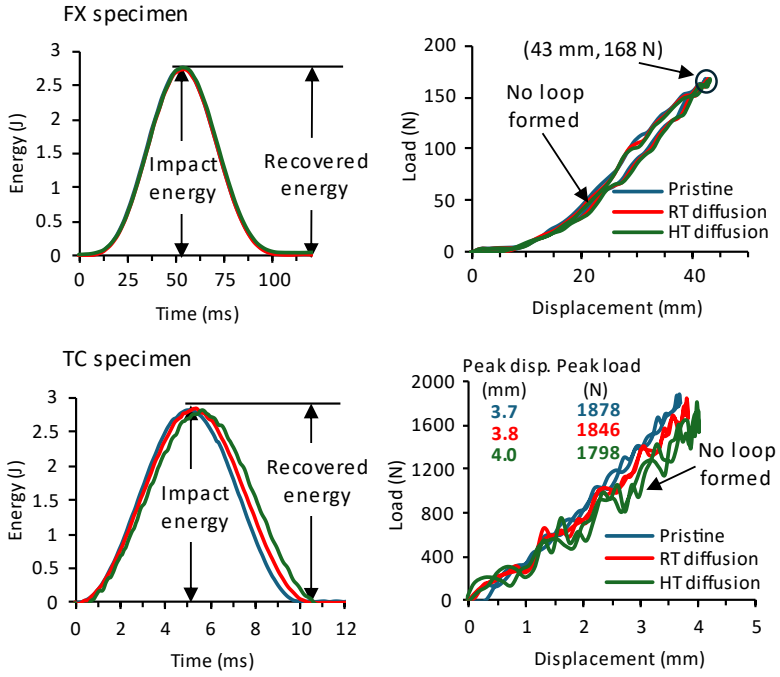

Fig. 11. Predicted energy-time and load-displacement responses of the epoxy specimens due to 3 J impact in pristine, room temperature (RT), and high temperature (HT) diffusion conditions.

6 Conclusion and Future Works

In this work, a sequentially coupled numerical framework was developed to investigate the application of two commercially available epoxy potting materials for underground wireless power transmission (WPT) systems. The framework successfully captured the effects of internal heat generation from the WPT system and long-term water diffusion-induced damage in the epoxy materials through low-velocity impact (LVI) simulations. The model predicted that under both room and high temperature diffusion conditions:

- The flexible specimen absorbed more water, leading to greater swelling compared to the rigid specimen.
- The structural performance of both epoxy materials was not significantly affected by diffusion-induced swelling.

The model prediction suggested that the flexible epoxy material is more suitable for protecting WPT components by reducing the likelihood of environmental aging and LVI damage. As part of future works, LVI tests will be performed on pristine and water-diffused epoxy specimens to validate the model prediction. Additionally, plastic properties and damage parameters will be incorporated into the model to predict the damage resulting from hydrothermal aging.

7 Acknowledgements

This work was supported in part by the National Science Foundation (NSF) Advancing Sustainability Through Powered Infrastructure for Roadway Electrification (ASPIRE) Engineering Research Center under Grant EEC-1941524.

References

1. Bi Z, Kan T, Mi CC, et al (2016) A review of wireless power transfer for electric vehicles: Prospects to enhance sustainable mobility. Appl Energy 179:413–425
2. Jones PT, Onar O (2014) Impact of Wireless Power Transfer in transportation: Future transportation enabler, or near term distraction. 2014 IEEE International Electric Vehicle Conference, IEVC 2014.
3. Dong X, Vuran MC (2013) Impacts of soil moisture on cognitive radio underground networks. 2013 1st International Black Sea Conference on Communications and Networking, BlackSeaCom 2013 222–227.
4. O'Malley G, Fu H (2012) Investigation of factors that influence creep corrosion - iNEMI project report. 2012 4th Electronic System-Integration Technology Conference, ESTC 2012.
5. Conseil H, Jellesen MS, Ambat R (2014) Experimental study of water absorption of electronic components and internal local temperature and humidity into electronic enclosure. Proceedings of the 16th Electronics Packaging Technology Conference, 355–359.
6. Shirangi MH, Fan XJ, Michel B (2010) Mechanism of Moisture Diffusion, Hygroscopic Swelling, and Adhesion Degradation in Epoxy Molding Compounds. Proceedings - 2008 International Symposium on Microelectronics, IMAPS 2008 29–69.
7. Staliulionis Z, Jabbari M, Hattel JH (2016) Moisture ingress into electronics enclosures under isothermal conditions. AIP Conf Proc 1738:30041.

8. Yu Q, Xiong R, Li C, Pecht MG (2019) Water-Resistant Smartphone Technologies. IEEE Access 7:42757–42773.
9. Niimi Y (2014) ECU Technologies from Components to ECU Configuration. Encyclopedia of Automotive Engineering 1–15.
10. Schuettler M, Schatz A, Ordonez JS, Stieglitz T (2011) Ensuring minimal humidity levels in hermetic implant housings. Proceedings of the Annual International Conference of the IEEE Engineering in Medicine and Biology Society, EMBS 2296–2299.
11. Baylakoğlu İ, Fortier A, Kyeong S, et al (2021) The detrimental effects of water on electronic devices. e-Prime - Advances in Electrical Engineering, Electronics and Energy 1:.
12. Liu SH, Shen MY, Kuan CF, et al (2019) Improving Thermal Stability of Polyurethane through the Addition of Hyperbranched Polysiloxane. Polymers 2019, Vol 11, 697 11:697.
13. Olson R (1989) Parylene conformal coatings and their applications for electronics. Proceedings of the Electrical/Electronics Insulation Conference 272–273.
14. Industrial Adhesive Chemistries: Epoxy, Urethane, Silicone. https://www.appli-tec.com/articles/epoxy-polyurethane-silicone-adhesives/. Accessed 13 May 2024
15. Alam S, Hassan MT, Merrel J, Lee J (2024) Comparative Analysis of Water-Induced Response in 3D-Printed SCF/ABS Composites under Controlled Diffusion. SAMPE Journal 60(4):16-24.
16. Maggana C, Pissis P, (1999) Water sorption and diffusion studies in an epoxy resin system. Journal of Polymer Science Part B: Polymer Physics, 37(11):1165-1182.
17. Niu YF, Yan Y, Yao JW (2021) Hygrothermal aging mechanism of carbon fiber/epoxy resin composites based on quantitative characterization of interface structure. Polym Test 94:107019.
18. Fan X, Zhang GQ, van Driel WD, Ernst LJ (2008) Interfacial delamination mechanisms during soldering reflow with moisture preconditioning. IEEE Transactions on Components and Packaging Technologies 31:252–259.
19. Lau JH, Lee SWR (2000) Temperature-Dependent Popcorning Analysis of Plastic Ball Grid Array Package During Solder Reflow With Fracture Mechanics Method. J Electron Packag 122:34–41.
20. van Driel WD, van Gils MAJ, Fan X, et al (2008) Driving mechanisms of delamination related reliability problems in exposed pad packages. In: IEEE Transactions on Components and Packaging Technologies. pp 260–268
21. Nayak RK, Mahato KK, Ray BC (2016) Water absorption behavior, mechanical and thermal properties of nano TiO2 enhanced glass fiber reinforced polymer composites. Compos Part A Appl Sci Manuf 90:736–747.
22. De'Nève B, Shanahan MER (1993) Water absorption by an epoxy resin and its effect on the mechanical properties and infra-red spectra. Polymer (Guildf) 34:5099–5105.
23. Fan XJ, Lee SWR, Han Q (2009) Experimental investigations and model study of moisture behaviors in polymeric materials. Microelectronics Reliability 49:861–871.
24. Toscano A, Pitarresi G, Scafidi M, et al (2016) Water diffusion and swelling stresses in highly crosslinked epoxy matrices. Polym Degrad Stab 133:255–263.
25. Thermally Conductive Epoxy. https://mgchemicals.com/products/potting-compounds/epoxy-potting/thermally-conductive-epoxy/. Accessed 4 Jul 2024
26. ASTM D570-98, Standard Test Method for Water Absorption of Plastics, ASTM International, West Conshohocken, PA, 1998
27. Abaqus/CAE User's Manual Abaqus 6.11 Abaqus/CAE User's Manual
28. Crank, John, "The Mathematics of Diffusion", *Oxford University Press*, 1975.
. Teverovsky A. Environmentally Induced Swelling and Shrinkage of Molding Compounds in PEMs. Greenbelt MD, NASA/GSFC. 2002.